Force Measurement Device for Semi-Submerged Bodies -Final Project Summary Report 2014

Sarah Louise Budd

University of New South Wales at the Australian Defence Force Academy

Submerged and semi-submerged bodies experience unique forces acting upon them. This thesis will experimentally investigate the drag and resultant forces acting on submerged and semi-submerged bodies with varying velocities and angles of attack. A sphere was used to calibrate the experimental test apparatus to ensure data collected was valid in comparison to historical data. A test apparatus was designed out of aluminium sections and a 1KN load cell was used to measure the forces acting on each of the test objects. The output from the load cell was averaged over 60 measured data points for each fixed velocity and angle of attack. The result, when converted into coefficient form, was a close match to historical data which implied the experimental test apparatus is accurate. It can then be used to explore the forces involved in more complex shapes in semi-submerged/ planning conditions. Data for a ski shape was taken and the result was an exponential Cd v Re curve which aligns with the graph for the drag equation as expected. Overall the results taken in tests with the experimental test apparatus align with theoretical and historical values which proves that the apparatus functions as intended and can be used as a method of measuring forces on submerged and semi-submerged objects in the future.

Contents

I. Introduction

A. Background

The main motivation for this project was the unfortunate accident (Fig 1), of the single-engine water bombing aircraft (VH-LIS) which crashed into Lake Liddell NSW in December 2007 (Australian Transport Safety Bureau, 2007). The modified Air Tractor aircraft was conducting test runs of a new concept; a ski-shaped water scoop fitted to the undercarriage of the aircraft aimed to allow for in-flight water reloading by skimming along the surface of a dam. On the second day of full-scale testing, the right ski, used to scoop water into the main tank, dug in to the lake, creating a pitching moment about the ski. This caused the aircraft to flip and crash into the lake. Unfortunately the pilot Colin Pay, who was also the pioneer of the innovative water collection system, was killed in this accident. Investigation and subsequent report of the accident revealed that there was no preliminary scale testing in the development of the ski system and the inaugural trial was a full scale test on the lake.

Figure 1: *Accident of Air Tractor, fitted with experimental water ski/scoop system.*

B. Aims

This project aims to design, build and calibrate a measurement system capable of collecting data for forces acting on submerged and semi-submerged simple geometry objects. The experimental test apparatus aims to provide a new method of data collection which can be compared with other methods by comparing the results plotted on a Cd v Re curve as is done in historical experiments.

II. Project Outline

A. Requirements

The main requirements for this project to be considered successful include;

1. A facility or means to simulate flowing water over the test object.
2. Access to the ADFA student workshop and funds to construct the test apparatus.
3. Suitable materials and environmental conditions.
4. Published theoretical or experimental data to make comparisons with.

B. Goals

This project has two primary goals which must be achieved in order for it to be deemed successful:

1. Design and build a test apparatus for the specific use of measuring forces on different test objects.
2. Calibrate the test apparatus and compare measured and theoretical data to determine the validity of the measurements.

C. Methodology

Experimental data will be collected for constant angle of attack and variable speed for three different test shapes; a submerged sphere, a submerged flat plate and planning ski/water scoop (a scale model of the ski fitted to the Air Tractor aircraft in figure 1.) The goal of the test apparatus is to measure force values that will re-validate existing theory and experimental data for simple geometry shapes. This will allow more research to be done in the field of high Reynolds number flow over bodies without the necessity of a water flume or other expensive setups.

D. Design

The basic design of the test apparatus involves two major sections of aluminium. A 2m long right-angle section will be welded at the end to a 0.8m vertical arm made of 2mm thick aluminium sections which bolt together to hold a 1KN load cell in position. Figure 2 shows a CATIA model of the test apparatus alongside images of the experimental setup.

Figure 2: CATIA *drawings of test apparatus (left) and experimental test setup for flat plate (right)*

i. The Testing Facility

Several testing configurations were considered but ultimately an apparatus was designed to fit onto a boat. The intent in choosing this testing method was that the apparatus would have the capacity to submerge the test object in water just outside its own wake whilst maintaining a constant angle of attack and variable speed. Using a Zodiac boat, (Figure 3), from the ADFA boat shed and conducting tests on Lake Burley Griffin proved the easiest and most cost effective solution. However this option created multiple external variables whilst trying to match environmental conditions on each run as well as errors in the boat speed and angle of attack.

Figure 3: *Zodiac Boat. Specifications: 0-15knots, on-board speed readout, inflatable rubber edges, adjustable pitch angle.*

ii. The Measurement System

The device chosen to measure the resultant force acting on the test object was an 'S' type, Precision Transducers Ltd, model AST100, tension load cell with a 100kg (1KN) capacity (Fig 4) (PT Global, n.d.). The load cell was calibrated in the UNSW@ADFA civil engineering laboratory to a 0.01% fs non-linearity. It was chosen for its robustness, longevity and high protection rating. Its (IP-67) protection rating means that its inbuilt electronic cables and connectors were totally protected against dust ingress and short periods of immersion in water, provided the exposure is short and the depth between 0.15m and 1m (IP Ingress Protection Ratings, n.d.). The output from the load cell will be collected through a data Vishay Micro-measurements data logger and converted to straight to a SD card or onto a laptop. The data logger showed a real time feed of the forces being measured. This proved useful in some of the test runs where a turn in weather conditions meant a rogue wave hit the flat plate and caused it to dig into the water. The load cell registered a 0.5kN force, half of the allowable limit of the cell.

Figure 4: *Precision Transducers, "S" type 1KN load cell*

The load cell was placed one third of the way from the bottom of the vertical arm so that it didn't experience high bending moments at faster speeds. A major concern with load cells is that they only work if the load is applied through its vertical axis. Force acting through the horizontal axis will create a shear force on the load cell which would ruin the strain gauge components. The test apparatus was built with this in mind, which was why the force was measured perpendicular to the main surface of the test shape. Figure 5, shows the direction the forces are acting. Since the load cell was built into the vertical arm it will only measure the total resultant force on the test object. The lift and drag forces on the test object can be found mathematically using sine and cosine relations as seen in figure 5.

The size and strength of the materials used to build the test rig were also a design consideration. The structure itself had to be made of a strong enough material that it wouldn't bend and deform under its own weight or the load of the water. Since the test object had to be held under the surface of the water outside the boat's wake the horizontal arm had to be at least 2m long and the vertical arm 80cm to reach the water's surface. The entire structure was made out of different sections of aluminium which were either bolted or welded together. Deflection and deformation were considered, resulting in horizontal arm being made of a right angle cross section, so that it didn't bend under its own weight over the 2m length. All other defections of the structure had a negligible effect on the total force measured and were ignored.

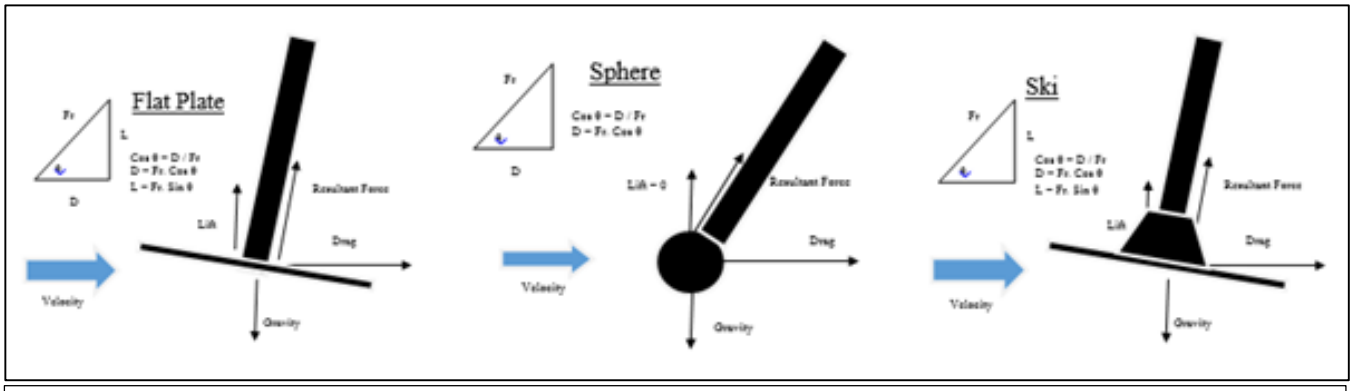

Figure 5: *Shows how to break the measured resultant force read by the load cell and convert it into lift and drag components.*

iii. Selection of Materials

Since simple materials and simple methods were desirable, the test apparatus was designed around easily obtainable and workable metal sections. The intent in the design of the apparatus was to use aluminium since it is an easy material to work with and has a low susceptibility to rusting. Milling qualifications and the ordering of specific materials is time consuming, which is the reason the design was focused around mainly bolt connections.

III. Theory

A. Sphere

Flows past objects encompass an extremely wide variety of fluid mechanics phenomena. For a given object, the characteristics of the flow depend on size, orientation, speed and fluid properties. Of the three simple geometry shapes tested, the test apparatus was calibrated using the sphere because there was so much data available to make comparisons. To calibrate the test apparatus it was important to recognize what effects overall drag as well as the flow characteristics of flow over a sphere.

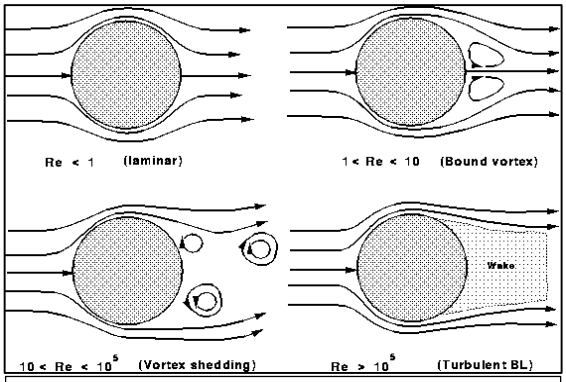

Figure 6: *Separation profiles over a sphere at varying Reynolds numbers.*

The Reynolds number represents the ratio of inertial and viscous effects in a flow. As a rule of thumb, Re>100 are dominated by inertial forces. At very high Reynolds numbers the flow has high inertia and can no longer follow the curved path around the rear of the body. This leads to separation and eventually the formation of a wake behind the object as seen in figure 6. At high Reynolds numbers the flow is considered turbulent and the profile has a wake at the trailing edge of the sphere (Southard, 2006). Drag on an object in a flow field is made up of two components; friction and pressure drag. Friction drag is directly related to shear stress while pressure drag is from the pressure difference caused by the object being placed in the flow field. At high Reynolds numbers, like those studied in this thesis, the pressure differential between the front and rear of the sphere accounts for the majority of the drag.

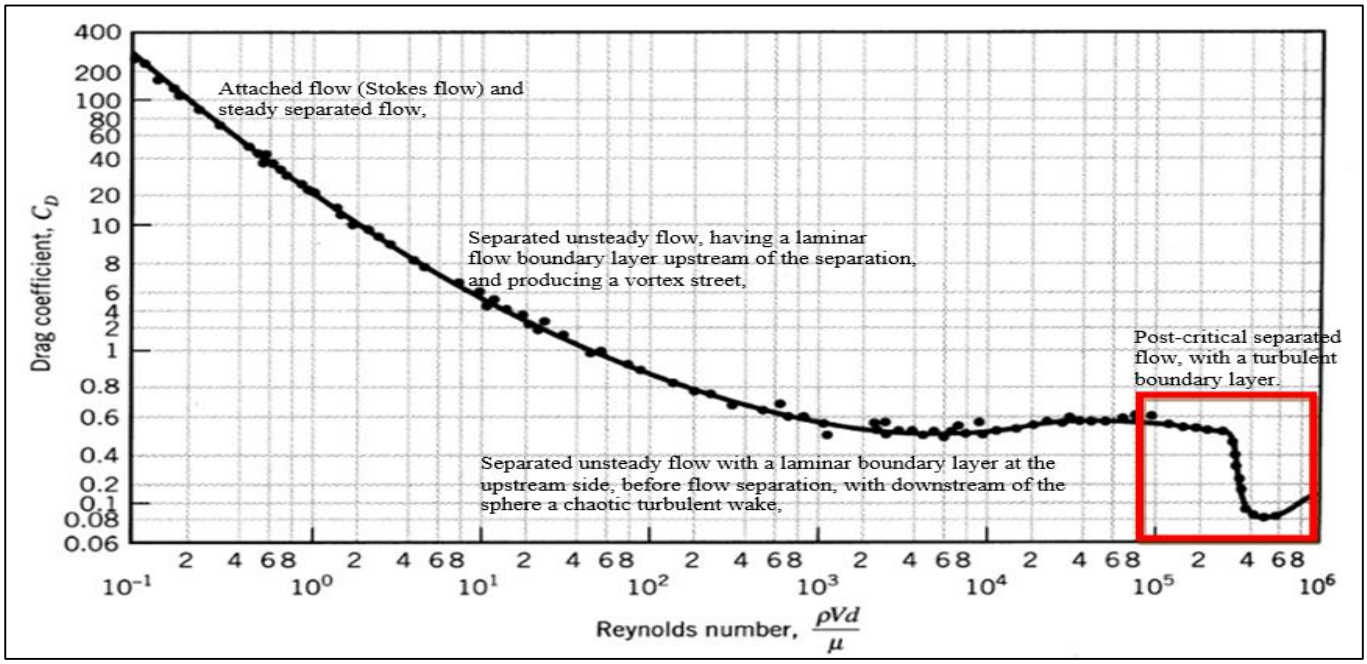

Figure 7: *Reynolds Number v Drag Coefficient graph. The highlighted section is the area of interest in this thesis*

Figure 7 shows the relationship between the drag coefficient and the Reynolds number. The speeds tested in this experiment have Reynolds numbers in the range of $(1.5x10^5) \leq Re \leq (8.6x10^5)$ which puts it in the highly turbulent, post critical flow with a turbulent boundary layer, range of the plot. The graph is derived from historical laboratory experiments. Each section indicates unique flow regimes and associated changes in the drag coefficient.

IV. Literature Review

A. Preceding Research

Majority of experiments testing drag coefficients on spheres occur at low Reynolds numbers where the flow is laminar. Turbulence, which occurs in flows at high Reynolds numbers, is not well understood by the scientific community, and as such mathematical models aren't available to predict the drag coefficients. Instead all values for this region ($Re>10^5$) are found experimentally. Since this thesis is working between $10^5<Re<10^6$, data must be compared with experimental results from papers rather than curve fit relations as would be done for laminar flow cases.

Achenbach wrote a paper in 1972 on the effects of high Reynolds number flows over spheres. He conducted numerous experiments in the Reynolds number range of $5 \times 10^4 < Re < 6 \times 10^6$, focusing on boundary layer separation and the dependence of friction forces on Reynolds numbers (Achenbach, Experiments on the flow past spheres at very high Reynolds numbers, 1972). Published experimental results for high Reynolds number flows from other authors include; (Bacon & Reid, 1924), and (Wieselsberger, 1922) who both conducted similar tests and obtained comparable results. Achenbach compared results from previous papers to his experiments and found that they deviated slightly (Fig 8) due to the differences in there experimental setup. Turbulence level of the flow, the effect of supports, surface roughness and flow velocity all have an effect on the output data. He makes note of the shape and trends of the experimental results, including the critical Reynolds number, $Re=3.7x10^5$, which corresponds to the lowest drag coefficient, also known as the drag crisis (Fig 8). Majority of the data collected over many years from numerous different setups all follow a similar trend line, which instills confidence in the correctness of the measured results.

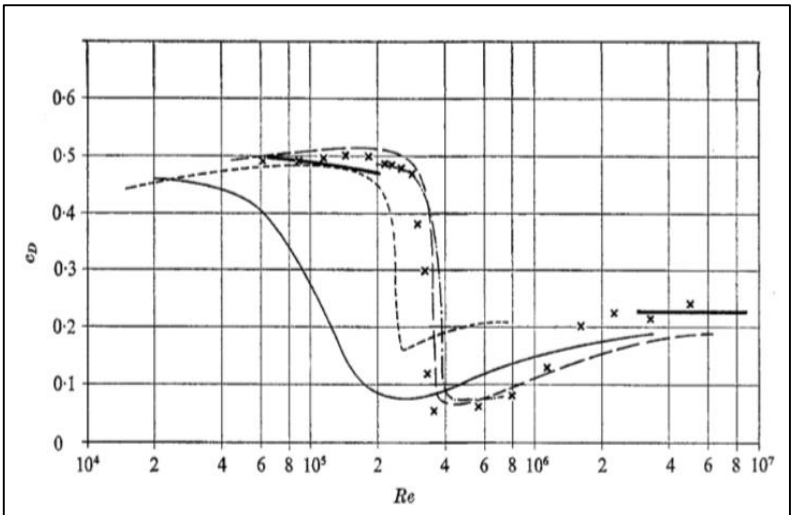

FIGURE 6. Drag coefficient of the sphere as a function of Reynolds number; comparison with literature. – – –, Wieselsberger (1922); ——, Bacon & Reid (1924); —·—, Millikan & Klein, free-flight (1933); ——, Maxworthy (1969). Present results: ——, from strain gauges; ×, from integration.

Figure 8: *paper reporting the Reynolds Number v Drag coefficient curve for high Reynolds number flows.*

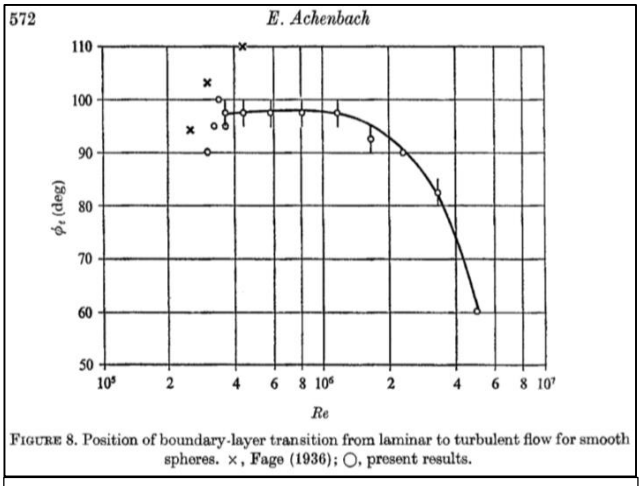

FIGURE 8. Position of boundary-layer transition from laminar to turbulent flow for smooth spheres. ×, Fage (1936); ○, present results.

Figure 9: *Achenbach's experimental results comparing Reynolds number to angle of separation.*

Achenbach also investigated boundary layer transitions and noted the relationship. As the Reynolds number increases, the location at which the flow separates varies.

Compared with a laminar profile, a turbulent boundary layer has a fuller velocity profile and remains attached for longer. At $Re>10^6$, the boundary layer becomes turbulent before separation takes place, and there is a sudden change in the flow pattern. Turbulent separation takes place toward the rear of the sphere, at angles illustrated in figure 9.

The wake becomes contracted compared to its size when the separation is laminar (Fig 6). Consequently the low pressure exerted on the surface of the sphere, within the separation region, acts over a smaller area. Also, the pressure itself in this region is not as low. The combined result of these two effects is a sudden drop in the drag coefficient, to a minimum of about C_D=0.1 (Achenbach, The effects of surface roughness and tunnel blockage on the flow past spheres, 1974). This is sometimes called the drag crisis seen in figure 10.

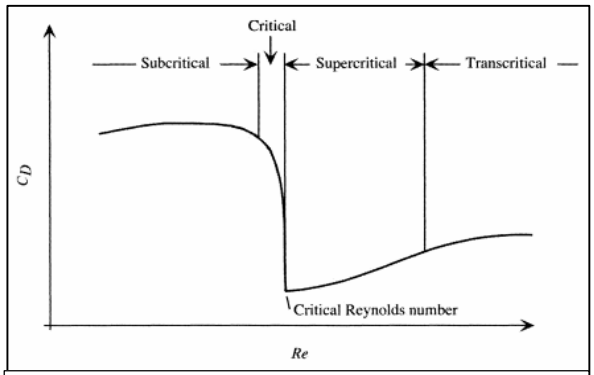

Figure 10: *Flow regimes of a sphere at high Reynolds numbers ($10^4<Re<10^6$).*

Achenbach published another paper on the effect of surface roughness (Achenbach, Vortex Shredding from Spheres, 1974). He studied the effects of surface roughness on flows past spheres, finding that as the surface roughness increases the critical Reynolds number decreases. Whilst at the same time the trans-critical drag coefficient rises. Achenbach wrote "Roughness elements distributed on the surface of a body in a fluid stream cause transition from laminar to turbulent flow if the disturbances generated by them are amplified. For bluff bodies without salient edges to fix the separation points, the premature onset of turbulence in the boundary layer causes a shift of the separation point and hence a change in the drag forces."

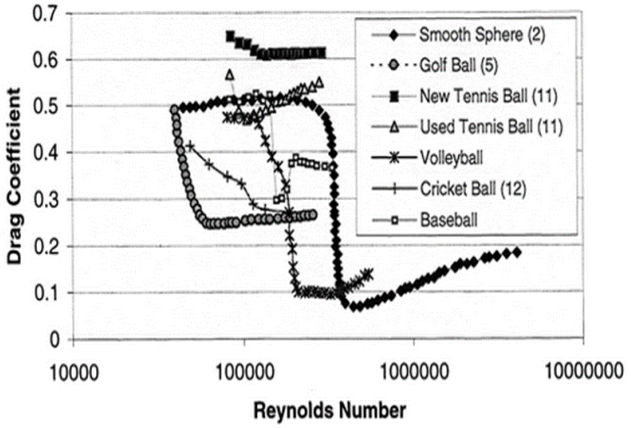

Figure 2: Drag coefficient versus Reynolds number for different sports balls. Volleyball data courtesy of Don Geister, Aerospace Department, University of Michigan.

Figure 11: *Effect of surface roughness on a Re v Cd plot for various sporting balls.*

Sports aerodynamicists Mehta and Pallis, studied the effect of surface roughness on different types of sporting balls, including a tennis ball used this thesis. Their intent was to verify Achenbach's surface roughness experiment using common sporting balls (Mehta & Pallis, 2001). You can see in figure 11 that the critical Reynolds number is shifted to the left in all non-smooth cases. Effectively, all sports balls have some sort of mechanism of tripping the laminar boundary layer using protuberance or surface roughness which forces them to transition earlier.

V. Experimental Results

A. Testing Plan

In order to determine the accuracy of the test apparatus it was first tested on a fully submerged sphere. The test sphere was made of a 16cm diameter tennis ball filled with fine grain cement and attached to the vertical arm of the test apparatus. A number of test runs were made for this shape at an angle of attack of 15 degrees. The speed was increased incrementally in factors of two from two to 12 knots with 60 data points taken for force at each speed. When gathered the data will be plotted on a Cd v Re graph and compared to historical examples. When proved accurate testing will begin on the flat plate and the ski and comparisons between expected and actual results will be made.

B. Controlled Variables

Since the testing for this thesis was done on a boat it was difficult to verify all the controlled variables in the same way that you could if you had done with a flume. Every effort was made to control variables in each of the tests. The speed was measured via a Garmin GPS unit which used satellite technology accurate to a square metre. It produced a speed readout every second and this was kept +/- 0.5 knots from the speed being tested. The depth of submersion for the flat plate and the sphere were not necessary since it was decided that the results would be more comparable with theory if they were fully submerged. For the ski however the depth of submersion was such that the entire flat section of the ski was skimming the surface and the front curved lip was above the water. A camera was mounted to the test apparatus and filmed each of the tests. This was then used to remove any data where the orientation of the shape was in question, such as it hitting a wave or rounding a corner. The angle of attack was the least controlled of the variables. It was measured using a spirit level against the test apparatus. When the boat was stationary or traveling up to 6 knots there was a +/- 1 degree error in this measurement. However, while the boat was traveling at greater speeds (above 6knots) the ability to check the angle was reduced. Though the accuracy of the angle is still 1 degree the fact that the boat was moving around so much and in some cases was hitting small waves the angle of attack varied in the region of +/-2 degrees. To this end, it was much easier to collect the data at slower speeds. This being said the data was collected over a 60 second period and the outliers were removed. This made the overall error much smaller.

C. Sphere Results

Several tests were done at varying speeds and the average of all data points was taken. Average forces had been recorded for speeds ranging from two to ten knots. From there this force (being the resultant force through the load cell) was broken into lift and drag forces using sine and cosine relations. Figure 12 is a plot of the measured drag forces against velocity. The theoretical drag force in this graph comes from data from historical experiments and the geometry of the test sphere. The orange line represents the drag that was actually measured and the dots represent the error at each point. It is evident that all the theoretical data lies within the bounds of the error bars, suggesting the test apparatus is accurately measuring the forces applied to the test sphere.

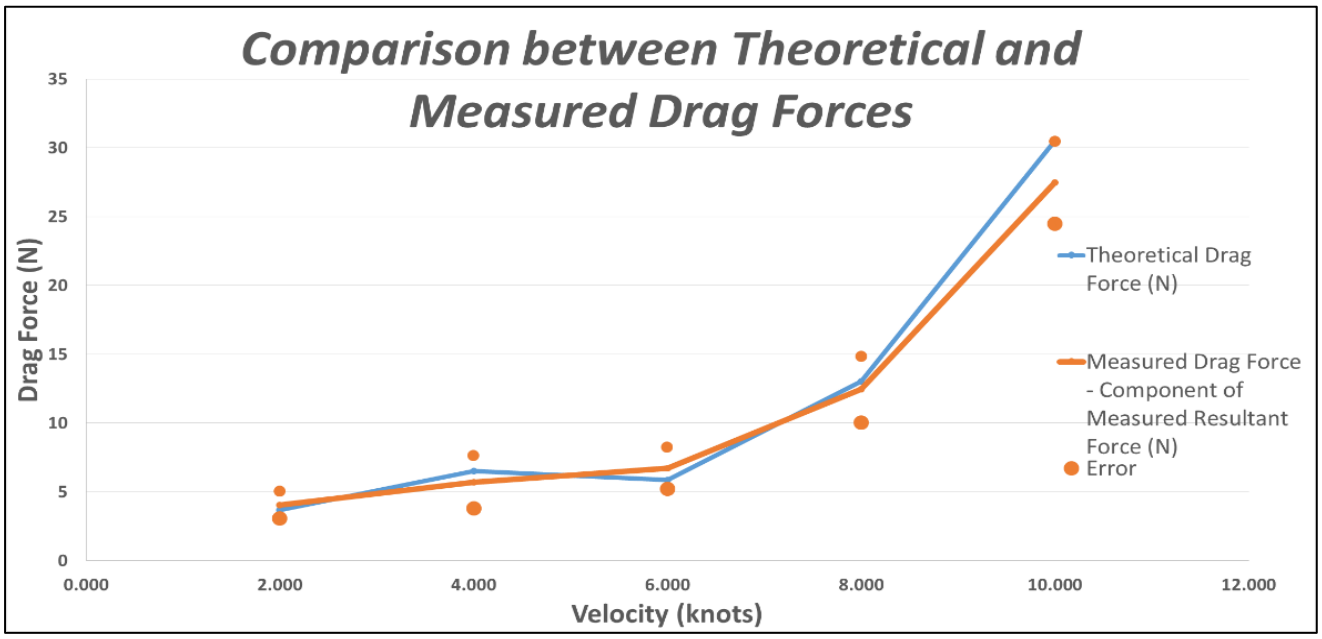

Figure 12: *Comparison between historical experimental data and time average measured drag forces on a sphere.*

The measured drag forces can then be converted into coefficient form and against the widely accepted Cd v Re graph in (Fig 7). Figure 13 shows the measured drag coefficient plotter against the theoretical Cd v Re plot for a smooth sphere.

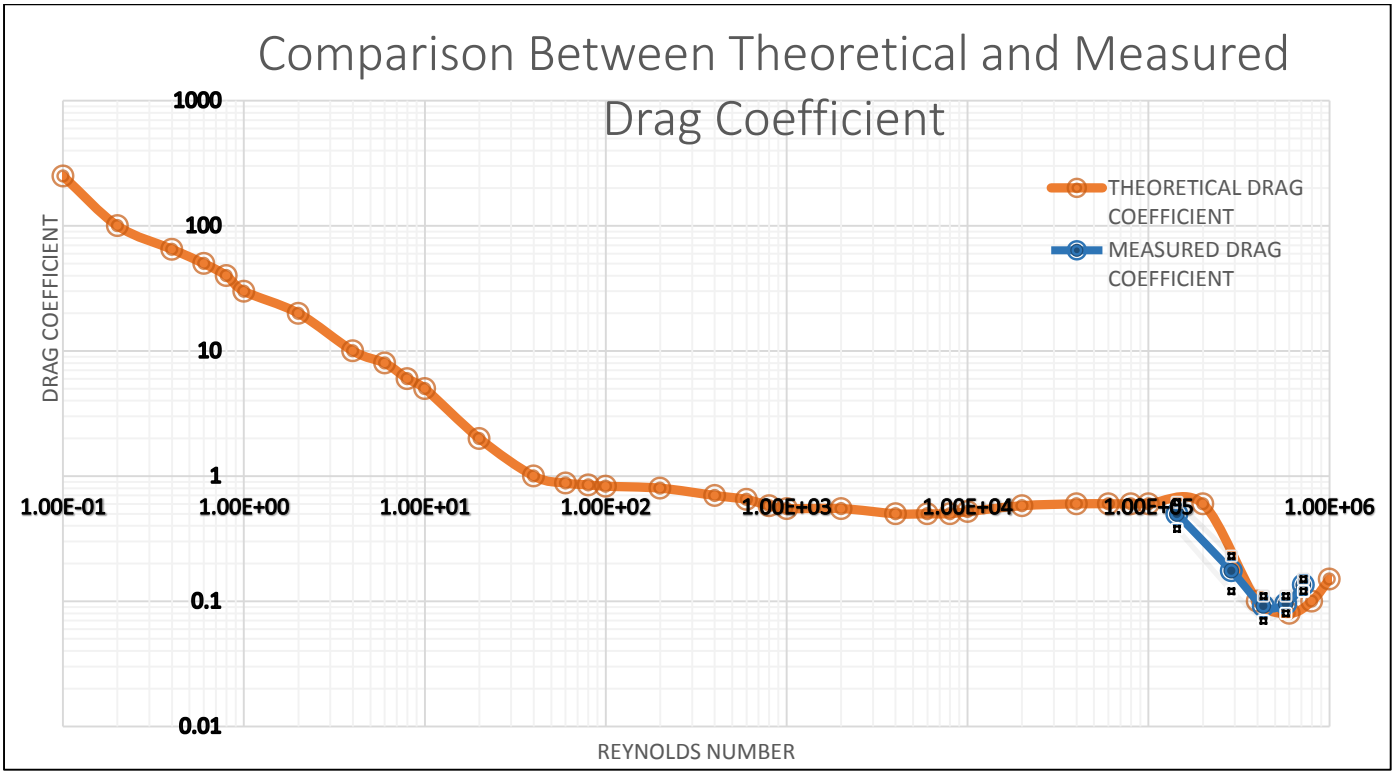

Figure 13: *Comparison of measured data to theoretical curve fit for drag coefficient v Reynolds number. Theoretical curve fit from Munson, Young, Okiishi and Huebsch, Fundamental of Fluid Mechanics Textbook*

In (Fig 13 and 14) the measured drag coefficient in blue reaches its drag crisis slightly before that of the smooth sphere. This is likely due to the surface roughness of the tested sphere. Figure 11 shows that the point of separation from laminar to turbulent occurs slightly earlier for the tennis ball coating. This it reflected in the measured data as the separation occurs earlier and has a higher minimum drag coefficient.

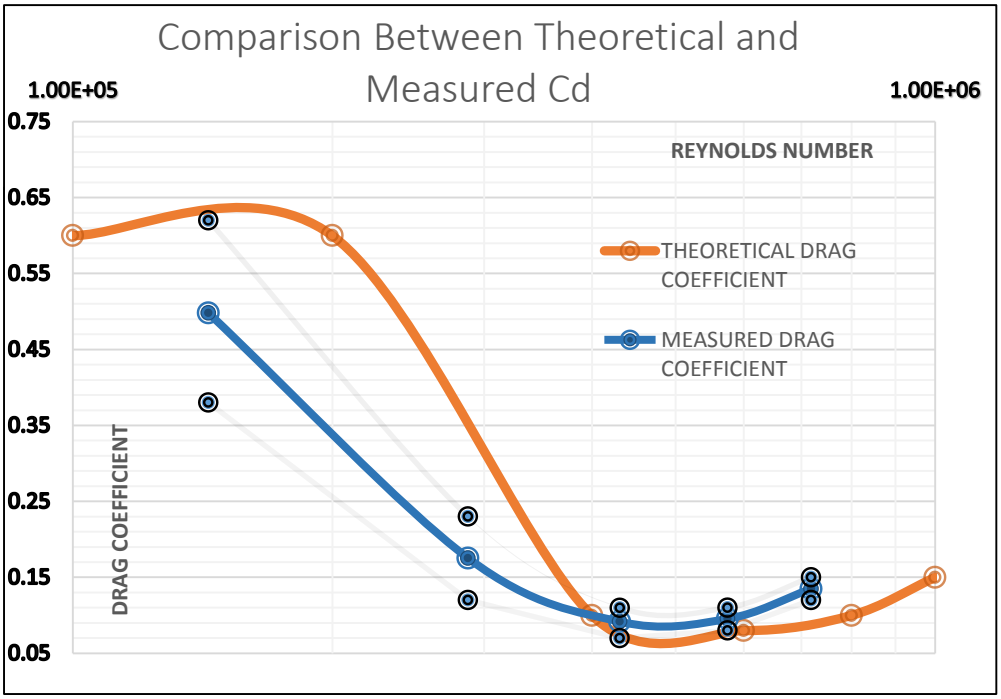

It is important to notice that the error gets smaller as the Reynolds number increases when plotted in coefficient form. On the graph of the actual measured forces (Fig 12) the error bars get larger. This is most likely caused by the fact that the confidence in the set angle of attack was reduced when the boat is traveling above six knots since the entire apparatus bouncing through the water.

Another important observation is that the critical Reynolds number is shifted to the left as is expected for a rough tennis ball replica of a sphere. The drag crisis, being lowest Cd, is higher than it would be for the theoretical smooth case which is aligns with the known effect surface roughness has on the drag on spheres as shown in figure 11.

D. Test Observations

Known flow profiles for the boundary layer have been established in theory. The profiles as identified in (Fig 6) are different for different Reynolds numbers. Even without a force measuring device, the approximate Reynolds number and associated drag coefficient can be seen from a visual inspection of the flow profile. (Fig 15 and 16) are representative of different speeds, one at 2 knots and the other at 10 knots. In both cases the flow is 100% turbulent and aligns with the theoretical picture of Re > 2 x 10^5 in (Fig 7) above. You can see that the flow separates between 90-120 degrees from the front stagnation point which aligns with the values Achenbach measured in (Fig 9) and has a highly turbulent wake.

The interference of the vertical arm of the measurement apparatus created its own wake at higher speeds and lead to an error in the final result. Therefore the drag on the vertical arm of the apparatus was likely to be small in comparison with the frontal area of the ball and can be ignored.

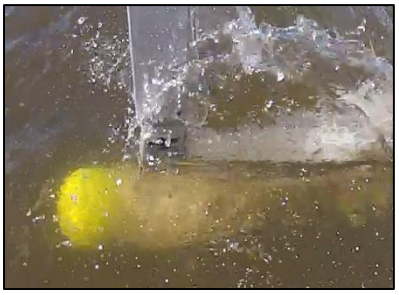

Figure 15: *Test Image at 2 knots*

Figure 16: *Test Image at 10 knots*

E. Error Analysis

As in all experiments there are several uncertainties that can be associated with the data gathered. Though all efforts were made to ensure the accuracy of the measured data, there are several obvious errors in the experimental design. There are several ways to calculate uncertainty in measurement. Firstly, the individual sources of error must be identified, then combined to give an overall figure. (Bell, 2001)

Identified uncertainties include;

- Angle of attack (spirit level) +/- 1deg
- Speed (Garmin GPS) +/-0.5knots
- Force measurement/ machine rounding +/- 0.005N
- Surface roughness +/- .02m
- Water temperature +/- 3^{o}C
- Environmental conditions (wind, waves) +/- 0.2

Since the errors are all of different units, they had to be non-dimensionalise in order to add them together to find the total error. The error margin on the results is likely to be quite high given the nature of the experiment, the reliance on environmental conditions and repeatability of test runs. The tests were all carried out in very similar conditions when the lake is calm so undulation of water surface was minimised.

$$\frac{Total\ Error}{Result} = \frac{AoA\ error}{AoA} + \frac{Speed\ error}{Speed} + \frac{Data\ Recording\ error}{Recorded\ Force}$$

For example for a sphere at 8 degrees angle of attack and 10 knots the experimental error would be;

$$\frac{Total\ Error}{Result} = \frac{1}{8} + \frac{0.5}{10} + \frac{0.05}{1.35} = 21\%$$

It can therefore be seen that the error in the force measurement for any point in this particular test was 21%. This means that the values for each measured data point is +/- 21% accurate. This formula also shows that the largest proportion of error comes from uncertainty in angle of attack as it has the largest uncertainty ratio. To refine this error the actual 50 point data package for each measured test condition needed to be analysed using the method below.

Error is the difference between the measured value and the 'true value' of a measurement (Ryerson University). Therefore most accurate results are found when averaging several readings. For each fixed angle of attack and speed the resultant force measured by the load cell was averaged over 50 or more data points. (Fig 17) shows the raw data for one of the test runs. The equations below detail how the error was determined.

$$Average\ or\ Mean = \bar{x} = \frac{1}{n}\sum_1^n x_i \qquad = 1.35\text{kg} \qquad = 13.5\text{N}$$

$$Standard\ Deviation = \sigma = \sqrt{\frac{\sum_1^n (x_i - \bar{x})^2}{n-1}} \qquad = 1.69$$

$$Standard\ Error = \sigma_m = \frac{\sigma}{\sqrt{n}} \qquad = 0.24kg \qquad = 2.4N$$

$$Final\ Error = x = \bar{x} \pm \sigma_m \qquad = 13.5\text{N} \pm 2.4\text{N}$$

Therefore the final error for this set of averaged data is 2.4N. This means that all data lies within a 17.7% deviation from the average. Note that the standard deviation for each data packet (i.e. at different speeds or angle of attacks) is different. This is reflected in the error margins on (Fig 12, 13 and 14) being of different magnitudes.

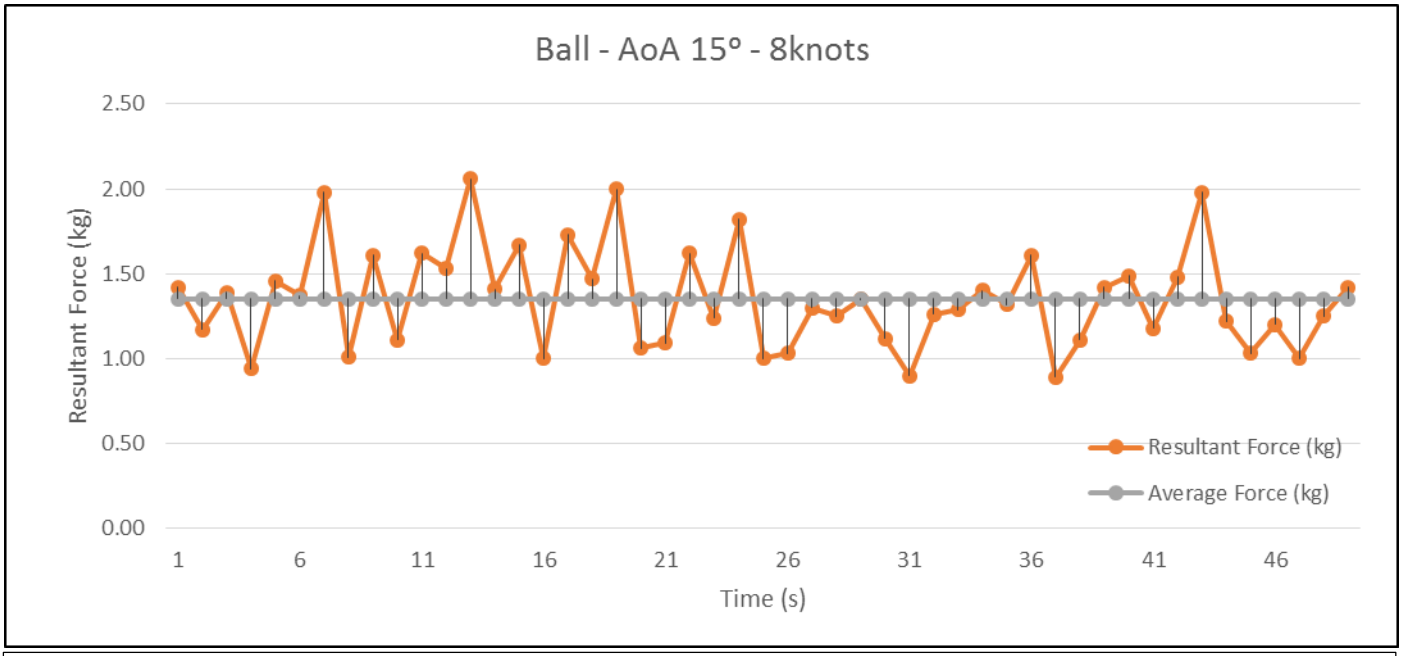

Figure 17: *Raw data collected for test run at 8 knots, 15 degrees angle of attack for the sphere.*

F. Ski Results

Since the water ski/scoop is an unusual shape there is no theoretical data available to compare it with. It was therefore expected that the test apparatus was calibrated prior to use. It was expected that the ski skimming along the surface behaved in a similar way to a flat plate.

Therefore the drag equation can be used to model the expected forces. It's expected that the drag profile at variable speeds will increase exponentially since the drag is a function of velocity squared (Munson, Young, Okiishi, & Huebsch, 2010) (Anderson, 2011).

$$D = \frac{Cd}{\frac{1}{2}\rho V^2 A}$$

Figure 18: *Test setup for the water ski/scoop*

Each trend line plotted is for a different fixed angle of attack at varying speeds. Note that the force measured seemed to be proportional to the angle of attack in that the higher the angle of attack the greater the drag force measured. This can

be seen in by the different size gaps between each trend line. This makes sense fundamentally since a higher angle of attack means the ski is presenting a larger frontal area to the flow which increase drag.

The results in (Fig 19) reflect the assumption that the drag follows an exponential profile, like that in the drag equation, since majority of the measured drag values either lie on the associated exponential curve or within the error bars of the exponential curve

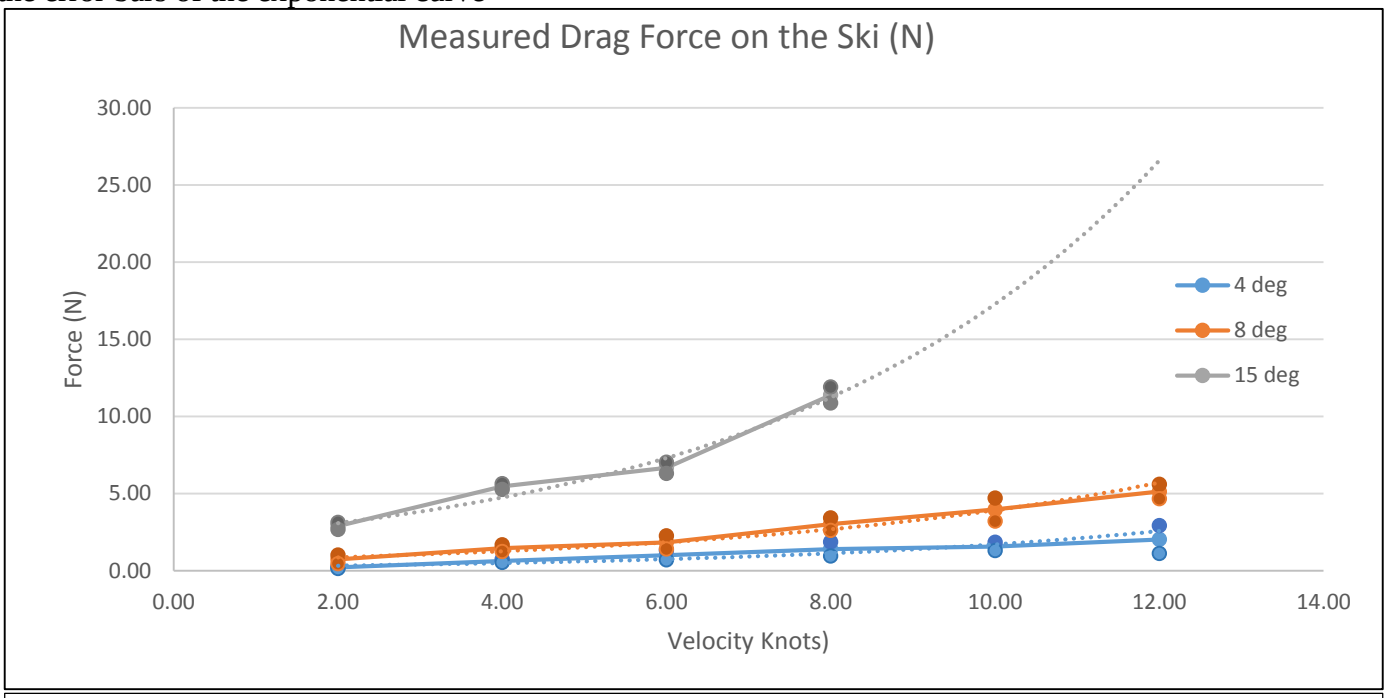

Figure 19: *Results of the drag measured on the ski with error bars and the expected exponential curve included.*

G. Flat Plate Results

Mid-way through the testing process it was decided to test a fully submerged flat plate, rather than the planning plate, since more information was available for flow effects in a single medium. The design of the test apparatus was such that the vertical arm wasn't long enough to fully submerge the flat plate without also submerging the load cell. Unfortunately the load cell was submerged for a short period, still within its operating limits, but stopped reading reasonable data. Flat plate data would have been very useful to compare to ski data to see how the difference in the unique ski design effects the overall force.

VI. Conclusions

The aim of this thesis was to design, build and calibrate a test apparatus capable of measuring forces on submerged and semi-submerged bodies. Validating existing data for drag on spheres using different methods which could be transferred to test the forces acting on other objects was of utmost importance. Several test facilities and methods were considered with the final method being a test apparatus (Fig 5) connected to a boat which held the test object submerged just outside the boats wake. Force data was found through experiment for 60 data points at each speed and angle of attack. The average of these 60 measured points was taken and converted from total resultant force to drag force and finally a drag coefficient. Through experimentation theoretical values for drag coefficients at varying Reynolds numbers (Fig 7) were verified. The closeness of the results measured by the test apparatus in comparison to theoretical values (Fig 13) instilled confidence in the test apparatus's accuracy. Factors for the slight difference in theoretical and measured drag coefficients including; surface roughness, flow separation and pressure distribution were all investigated. The most likely cause of the difference being the effect of surface roughness which was shown from theoretical data in (Fig 11). Once the test apparatus was calibrated and its accuracy proved, it was used to determine the forces on unusual shapes like the experimental water ski/ scoop fitted to the Air Tractor. The results found for the ski

were as expected. They fitted an expected profile which corresponds to the drag equation, being a function of velocity squared. This thesis proved that it is possible to design a relatively cheap, and simple apparatus capable of measuring forces on a submerged or semi-submerged planning object to a high degree of accuracy.

VII. Recommendations

Adjustments need to be made to the test apparatus in order to be able to measure forces acting on a fully submerged flat plate. It's suggested that the lower section of the vertical arm be extended by 20cm to allow sufficient room for the plate to be submerged without also submerging the load cell. Flat plate data would be extremely valuable when directly comparing the safety and reliability of the ski. The data would be a useful comparison as it would highlight the significance the shape of the ski plays on the forces exerted.

It's also recommended that more data points be taken for each of the test objects. For the sphere testing this will mean that the actual critical Reynolds number, where the drag coefficient rapidly declines, and the drag crisis, the point of lowest drag coefficient could be identified with a greater accuracy. For the ski tests, more data points could be taken for each angle of attack, in addition to a wider variance in the angle of attacks to reinforce the current exponential trend lines.

References

Achenbach, E. (1968). Distribution of local pressure and skin friction around a circular cylinder in cross-flow up to Re = 5X10^6. *Journal of Fluid Mechanics*, 625-639.

Achenbach, E. (1972). Experiments on the flow past spheres at very high Reynolds numbers. *Journal of Fluid Mechanics, 54*(3), 565-575.

Achenbach, E. (1974). The effects of surface roughness and tunnel blockage on the flow past spheres. *Journal of Fluid Mechanics*, 113-125.

Achenbach, E. (1974). Vortex Shredding from Spheres. *Journal of Fluid Mechanics*, 209-221.

Anderson, J. (2011). *Fundamentals of Aerodynamics* (5 ed.). New York: McGraw-Hill.

Australian Transport Safety Bureau. (2007). *Controlled flight into water Lake Liddell, NSW-7 December 2007 VH-LIS Air Tractor Inc At-802.* Sydney: Australian Transport Safety Bureau. Retrieved from Australian Transport Safety: http://www.atsb.gov.au/publications/investigation_reports/media/2007/AAIR/pdf/AO2007066.pdf

Bacon, D. L., & Reid, E. G. (1924). *Report 185 - The Resistance of Spheres in Wind Tunnels and in Air.* National Advisory Committee for Aeronautics.

Bell, S. (2001). A Beginner's Guide to Uncertainty of Measurement. *Measurement Good Practice Guide, 11*(2).

Cimbala, J. M. (2012). *Drag on Spheres.* Penn State: Penn State University.

Howard, C. (2013). *Guide to the Measurement of Force.* UK: Institute of Measurement and Control. Retrieved from The Institute of Measurement and Control: http://www.npl.co.uk/upload/pdf/forceguide.pdf

IP Ingress Protection Ratings. (n.d.). Retrieved from IP Ingress Protection Ratings: http://www.engineeringtoolbox.com/ip-ingress-protection-d_452.html.

Klaka, K., Penrose, J. D., Horsley, M. R., & Renilson, M. R. (2005). Hydrodynamic tests on a fixed plate in uniform flow. *Experimental Thermal and Fluid Science*, 131-139.

Langan, J. F. (2014). *The Continuity Equation, the Reynolds Number, the Froude Number.* Retrieved from Yale-New Haven Teachers Institute: http://www.cis.yale.edu/ynhti/curriculum/units/1988/6/88.06.04.x.html

Mehta, R., & Pallis, J. M. (2001). Sports Ball Aerodynamics: Effects of Velocity, Spin and Surface Roughness. *Materials and Science in Sports*, 185-197.

Munson, B., Young, D., Okiishi, T., & Huebsch, W. (2010). *Fundamentals of Fluid Mechanics* (6 ed.). Asia: John Wiley & Sons (Asia) Pte Ltd.

PT Global. (n.d.). *AST S-Type Tension-Compression.* Retrieved from PT Global: http://www.ptglobal.com/category/47-ast-s-type-tensioncompression.html.

Ryerson University. (n.d.). *Introduction to Errors and Error Analysis.* Retrieved from Ryerson University Physics: http://www.physics.ryerson.ca/sites/default/files/u3/2011/04/Labs-IntroToErrorsFinal.pdf

Southard, J. (2006). *Chapter 3: Flow Past a Sphere II: Stokes' Law, The Bernoulli Equation, Turbulence, Boundary Layers, Flow Separation.* Retrieved from MIT Open Courseware: http://ocw.mit.edu/courses/earth-atmospheric-and-planetary-sciences/12-090-introduction-to-fluid-motions-sediment-transport-and-current-generated-sedimentary-structures-fall-2006/course-textbook/ch3.pdf

Wieselsberger, C. (1922). *Technical Note Number 84: New Data on the Laws of Fluid Resistance.* National Advisory Committee of Aeronautics.